J. Biomed. Eng. Res.
Vol. 21, No. 2, 119-127, 2000

CCD를 이용한 전자포탈영상장치의 엑스선 계측기 특성에 관한 연구

정용현* · 김호경* · 조규성* · 안성규* · 이형구** · 윤세철***

*한국과학기술원 원자력공학과, **가톨릭대학교 의과대학 의공학교실,
***가톨릭대학교 의과대학 방사선과

(2000년 1월 11일 접수, 2000년 2월 26일 채택)

Characterization of X-ray Detector for CCD-based Electronic Portal Imaging Device

Y.H. Chung , H.K. Kim, G.S. Cho, S.K. Ahn, H.K. Lee*, S.C. Yoon**

*Department of Nuclear Engineering, Korea Advanced Institute of Science and Technology,
373-1 Kusong-dong, Yusong-gu, Taejon 305-701, Korea
**Department of Biomedical Engineering and ***Department of Radiation Oncology,
Catholic University Medical College, 505 Banpo-dong, Seocho-gu, Seoul 137-040, Korea

(Received January 11, 2000. Accepted February 26, 2000)

요 약 : 금속판/형광스크린 계측기와 CCD 카메라를 이용한 방사선영상장치가 현재 전자포탈영상에 널리 쓰이고 있다. 이 장치의 효율적인 영상획득을 위해 계측효율이 좋고, 공간분해능이 뛰어난 금속판/형광스크린 계측기의 두께를 최적화할 필요가 있었다. 이 논문에서는 금속판과 형광스크린의 두께가 계측효율과 공간분해능에 미치는 영향이 연구되었다. 이 결과는 치료 엑스선 영상장치에 쓰일 수 있는 금속판/형광스크린 계측기의 최적화된 두께를 결정하는 데 쓰일 수 있다. 몬테칼로 방법을 이용하여 계산한6 MV 선형가속기에서 발생되는 엑스선의 에너지 스펙트럼을 바탕으로, 여러 가지 두께의 금속판/형광스크린에 대하여 계측효율과 공간분해능을 계산하였고, 이를 실험을 통해 검증하였다. 계측효율은 입사된 엑스선의 에너지가 형광스크린에 흡수된 비율로 계산되며, 공간분해능은 흡수된 에너지의 공간 분포를 통해 계산되었다. 계측효율은 금속판의 두께에 의해, 공간분해능은 형광스크린의 두께에 의해 결정될 수 있음을 본 연구를 통해 알 수 있었다. 더불어 계측효율과 공간분해능은 형광스크린의 두께에 대하여 서로 보상 (trade-off) 관계에 있음을 계산과 측정결과를 통해 확인할 수 있었고, 이로써 특정이용에 관련된 금속판/형광스크린 계측기의 최적화된 두께를 산출할 수 있게 되었다. 계산을 바탕으로 CCD를 이용한 전자포탈영상장치의 시작품을 설계 및 제작하였고 팬텀을 이용하여 영상을 얻었다. 단일 프레임 영상은 노이즈가 많으나, 프레임 평균 방법을 이용하여 영상의 질을 향상시킬 수 있었다.

Abstract : A combination of the metal plate/phosphor screen with a CCD camera is the most popular x-ray detector system among various electronic portal imaging devices (EPIDs). There is a need to optimize the thickness of the metal plate/phosphor screen with high detection efficiency and high spatial resolution for effective transferring of anatomical information. In this study, the thickness dependency on the detection efficiency and the spatial resolution of the metal plate/phosphor screen was investigated by calculation and measurement. It was found that the detection efficiency was mainly determined by the thickness of metal plate, while the spatial resolution was mainly determined by the thickness of phosphor screen. It was also revealed that the detection efficiency and the spatial resolution have trade-off in term of the thickness of the phosphor screen. As the phosphor thickness increases, the detection efficiency increases but the spatial resolution decreases. The curve illustrating the trade-off between the detection efficiency and the spatial resolution of the metal

통신저자 : 정용현, (305-701) 대전시 유성구 구성동 373-1 한국과학기술원 원자력공학과
Tel. (042)869-3861, Fax. (042)869-3810
E-mail. yhchung@cais.kaist.ac.kr

INTRODUCTION

Cancer is one of the leading causes of death and a

plate/phosphor screen detector was obtained as a function of the phosphor thickness. Based on the calculations, a prototype CCD-based EPID was developed and then tested by acquiring phantom images for 6 MV x-ray beam.
Key words : Portal Image, EPID, Bremsstrahlung Spectrum, detection Efficiency, Spatial resolution, Frame averaging

disease that reduces the quality of life in elderly population. Radiation therapy is the most common method of controlling cancer among the several treatment options for cancer. The goal of radiation therapy is to deliver a prescribed dose as accurately as possible to a tumor region while minimizing the dose distribution to the neighboring normal tissues[1]. The standard course of treatment is divided into daily fraction of about 200 cGy dose, delivered over a period of 25~35 days for a total of 5000 to 7000 cGy cumulative dose[2]. Because of daily treatment, discrepancies in field placement occur frequently, such as patient movement, improper placement of shielding blocks, shifting of skin marks relative to internal anatomy and incorrect beam alignment[3]. As a result, recommendations by the International Commission on Radiation Units (ICRU) suggest that the accuracy in dose delivery should be ±5%[4]. For achieving this accuracy, the methods to reduce the frequency of discrepancies of field placement by frequent monitoring of patient positioning are developed, known as portal imaging. Portal imaging is a process to form an image of the patient during radiation treatment for ensuring that the correct region of the patient receives the radiation therapy and that the surrounding tissues are spared.

Currently, the most commonly used portal imaging method employs a radiographic film placed in contact with a metal plate. Unfortunately, these film images suffer from many disadvantages, such as low image quality, fixed display contrast, limited dynamic range and time delay due to film development[5]. The number of alternative detectors, known as electronic portal imaging device (EPID), have been developed, and each detector overcomes some of these limitations. The digital images not only open up possibilities for quantitative comparison with simulator images, but can also be processed to overcome poor contrast. And imaging can be performed in real-time. The video camera or CCD-based EPID is still the most popular detector system among various EPIDs. [5-8] (Fig.1) The x-ray detector consists of a metal plate and a phosphor screen. The metal plate generates high energy electrons when irradiated by therapeutic x-ray with energy in order of 4~25MV. And the phosphor screen converts electrons into visible light and the light diffuses through the screen and exits the rear surface of the x-ray detector which is viewed by video camera via a 45 mirror. The video signal is digitized and the digitized image can be viewed on a monitor. As a metal plate which acts a build-up region, brass, steel and copper with the range of 1~2.25mm in thickness are commercially used[8-9]. In the case of phosphor screen, a terbium doped gadolinium oxysulfide (Gd_2O_2S:Tb) screen which is commonly applied to diagnostic radiology, with the range of 150~500mg/cm^2 in coverage is used [8-9]. Metal plate/phosphor screen is largely responsible for the total performance of the video camera-based EPID because it is the first stage of transferring an anatomical information in the image chains of system. Therefore the optimal design of the metal plate/phosphor screen as an x-ray detector for portal imaging is needed. Two quantities, such as detection efficiency and spatial resolution, are considered as a touchstone of good performance. In this study the megavoltage x-ray spectrum from 6 MV linear accelerator (LINAC) and the characteristics of various combinations in thickness of the metal plate and the phosphor screen have been investigated by calculation and measurement. This result can be used to determine the optimal thickness of metal plate and phosphor screen for specific application. Finally, prototype CCD camera-based EPID was developed and images were acquired

MATERIALS AND METHODS

1. X-ray Beam from Clinical LINAC

For the treatment of deep-seated tumors, megavoltage x-rays, typically in the range of 4 to 25MV, are required. LINAC is currently the most popular device for this application[10]. The energy spectrum of bremsstrahlung x-ray produced by the clinical LINAC is difficult to measure directly because detectors sensitive to photon energy cannot be used in the high photon flux produced by the accelerator. The flux is not adjustable and placing attenuators in the beam alters the spectrum. In order to obtain the bremsstrahlung spectrum from LINAC, Monte Carlo N-Particle, version 4B (MCNP4B) code[13] was used. The simulation geometry and dimensions of LINAC were designed based on the accurate geometrical data of 6MV LINAC (Siemens, Mevatron KD) to match the actual experimental setup. This consisted of an electron beam, a shielded and water-cooled gold target, a stainless

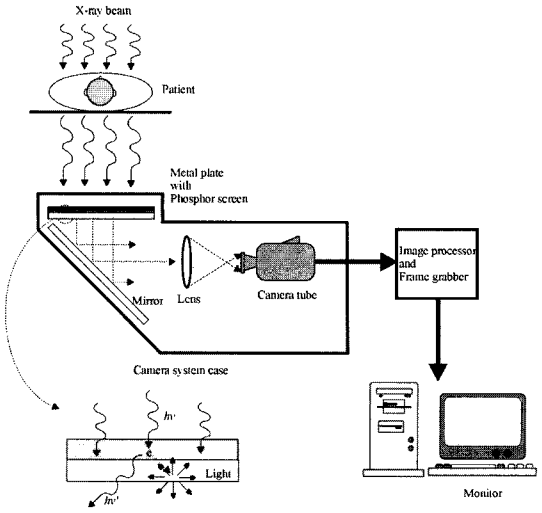

그림 1. 비데오 카메라를 이용한 전자포탈영상장치
Fig. 1. Schematic diagram of video camera-based EPID

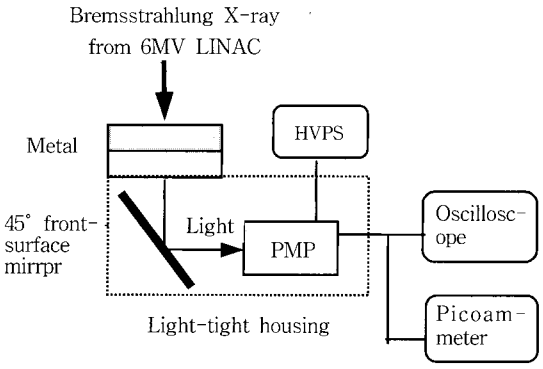

그림 2. 광량측정 시스템
Fig. 2. A schematic diagram of light-yield measurement system

steel flattening filter and ion chambers. For the incident electron beam, a 5-deg cone-shaped with kinetic energy of 5.58MeV, incident perpendicularly on the target was considered. Electrons were followed to a cut-off kinetic energy of 0.5MeV. This is sufficient, as the bremsstrahlung radiation yield of mono-energetic electrons in gold target with kinetic energies below 0.5MeV is less than 5.3%. The number of emerging photons from 5,000,000 histories were collected into ten energy bins, each of width 0.558 MeV, if they landed in a circular region of radius 4.375cm about the central axis at a distance 100cm from the target. The energy spectrum was computed by multiplying the number of photons in a given bin by the energy at the center of the bin.

To confirm the simulation result, Schiff spectrum was also calculated using the following equation[11], this is a relatively simple analytical form and has been used extensively for estimating the spectrum shape from a high energy accelerator.

$$\Gamma_{Schiff}(E_0, h\nu) = 8\left[2\left(1-\frac{h\nu}{E_0}\right)(\ln\varepsilon - 1) + \left(\frac{h\nu}{E_0}\right)^2\left(\ln\varepsilon - \frac{1}{2}\right)\right] \quad \text{(Eq. 1.1)}$$

$$\varepsilon = \left[\left(\frac{\mu/h\nu}{2E_0E}\right)^2 + \left(\frac{Z^{\frac{1}{3}}}{C}\right)^2\right]^{-\frac{1}{2}} \quad \text{(Eq. 1.2)}$$

where

E_0 : total energy of incident electron [MeV]
E : scattered electron total energy [MeV]
$h\nu$: bremsstrahlung photon energy [MeV]
μ : rest energy of electron [0.511MeV]
Z : atomic number of target material
C : dimensionless constant [111]

The Schiff spectrum presented here neglects several effects that contribute to the actual energy spectrum of LINAC, such as the electron energy spectrum within the target, Compton scattering of bremsstrahlung photons in the target or flattening filter, and scattering from collimator etc.

2. Detection Efficiency of X-ray Detector

In this study, the detection efficiency is defined as the total absorbed energy in the phosphor screen per incident x-ray. Since the number of optical photons generated is directly proportional to the total absorbed energy in a given phosphor screen. In order to determine the energy absorption within the phosphor screen, MCNP4B code [13] was used. In this study, the x-ray detector was simply modeled, which consisted of copper plate (0~50mm) in contact with Gd_2O_2S layer (0.1~5mm), with 20cm in radius. Despite of complexity of phosphor screen material composition, the density of Gd_2O_2S, which is assumed to be homogeneous mono-layer, was reduced to 3.67g/cm^3 accounting for polyurethane polymer-binder and small air pockets within a realistic phosphor layer[9,14]. For the incident x-ray beam, a pencil beam with bremsstrahlung spectrum as calculated in the above section, incident perpendicularly on the x-ray detector was considered. Locally distributed energy absorption was estimated in cubic cells of phosphor layer in Monte Carlo simulation. The total absorbed energy was computed by adding the

absorbed energy in a given cell.

To confirm the above calculation result, the system to measure the light output from metal plate/phosphor screen was developed. (Fig.2) It has a1 35mg/cm^2-coverage Gd_2O_2S (Lanex fast back screen, Eastman Kodak) attached onto a copper plate (0~50mm) as the x-ray detector. The detector is then optically coupled with PMT (Hamamatsu, PMT R5506) by an aluminum-coated, front-surface mirror with 45° inclined angle. The detector, mirror and PMT were placed in a light-tightened housing. The electronic signal from PMT is amplified by the current to voltage conversion amplifier (Hamamatsu, C1053-03) and then measured by both the pico-ammeter (Keithley, 485) and the oscilloscope. All experimental measurements were performed for the 6MV x-ray beam from LINAC (Siemens, Mevatron KD) at 300 MU/min and 100 cm SSD.

3. Spatial Resolution of X-ray Detector

To fully characterize the detector behavior it is necessary to have a model of optical photon transport out of the phosphor screen. The spatial resolution is defined by the full width at half maximum (FWHM) of a point spread function, which is the distribution of the optical photon-flux over the surface of the phosphor screen opposite to metal side. It is assumed that the optical photon generated in the center of a small cubic box of which total intensity is proportional to the total absorbed energy in the box and then propagates isotropically. Since the optical photon absorption-length (~4cm) in Gd_2O_2S[9] is sufficiently larger rather than the thicknesses of the generic Gd_2O_2S considered in this study, the attenuation of optical photons in the phosphor screen is neglected. In addition, the reflectance of the metal surface at the back of screen is also neglected because the light yield is not very sensitive to its value as described in [9]. The optical photon-flux collected over the solid angle of a rectangular pixel of size $2X \times 2Y$ can be expressed by [15-17] ,

$$P(z) = \int_{-Y}^{Y} \int_{-X}^{X} \frac{N_{opt}}{4\pi} \times \frac{z}{\left(x^2 + y^2 + z^2\right)^{3/2}} dxdy \qquad \text{(Eq.3.1)}$$

where x, y and z are 2-dimensional coordinates of the end-sided phosphor screen and distance to the light source, respectively. N_{opt} is the number of photons generated at which the x-ray energy is absorbed within phosphor screen and can be calculated by

$$N_{opt} = \varepsilon \times \frac{E_{abs}}{E_{opt}} \qquad \text{(Eq. 3.2)}$$

In Eq. 3.2, ε is the intrinsic conversion efficiency in the range of 15~20% [18-19], E_{opt} and E_{abs} are the optical photon energy (2.28eV for 545nm wavelength from Gd_2O_2S:Tb) and the locally absorbed energy within phosphor screen from the secondary fast electrons, respectively.

Locally distributed energy absorption was estimated in $100 \times 100 \times 100 \mu m^3$ cubic cell of phosphor layer by Monte Carlo simulation as described in the previous section. Then, the center point of the cell was assumed to be the representative position as the optical photon-source point. Based on the Monte Carlo simulated spatial distribution of energy absorption, the distribution of optical photon flux collected by $10 \times 10 \mu m^2$ pixel area as a function of pixel position on the free surface of the phosphor screen was calculated by Eq. 3.1 and Eq. 3.2 using a hand-made C program. To confirm the calculated spatial resolution, the experimental measurement was carried out. The line spread function is equal to the integral of the point spread function and the derivative of the edge spread function[20]. To determine the edge spread function of metal plate/phosphor screen, a density profile of a film across an edge was measured. A lead block with dimensions of $20 \times 10 \times 5cm^3$ was placed on a film cassette and across half of the x-ray field of 6 MV LINAC (Siemens, Mevatron KD) with 167cm SSD. The 135mg/cm^2-coverage Lanex screen attached onto a 2mm-thick copper plate was placed in the film cassette with the phosphor layer of the detector in contact with the portal film (Kodak, X-Omat V film) which is commonly used for the therapy verification. The film was exposed by the x-ray intensity of 50 MU (Monitor Unit, 1MU may be calibrated to equal 1 cGy at 100cm SSD for a $10 \times 10 \mu m^2$ field size at 5cm-depth in water). Therefore, the film recorded the edge spread function of the metal plate/phosphor screen detector while negligibly influencing the spread. The shape of the edge spread functions were measured with film digitizer passing through the image of the edge, perpendicular to the edge length. Thirty scans were made and these scans were averaged together to reduce uncertainty in the final estimation of the edge spread function.

4. Prototype CCD-based EPID

In order to capture the therapeutic x-ray images, a

prototype CCD-based EPID that consists of the metal plate/phosphor screen detector and CCD camera have been developed based on the calculation results. As an x-ray detector, the Lanex screen with 135mg/cm^2 coverage bonded onto a 2mm-thick copper plate is used. The detector is viewed by a CCD camera with a field of view (FOV) of 20×20cm^2 using a 45 inclined aluminum-coated, first-surface mirror. Samsung BW-2301ED operated by the interlaced scanning mode was used as a CCD camera with the 6~12mm zooming c-mount lens. These all the components were placed in the light tightened housing. The PCI-1408 ImaQ board (National Instrument) as a frame grabber was used for data acquisition. For the 6 MV x-ray beam from LINAC (Siemens, Mevatron KD) at 300MU/min and 100cm SSD, all measurements were performed with the humanoid head phantom. (Fig. 3)

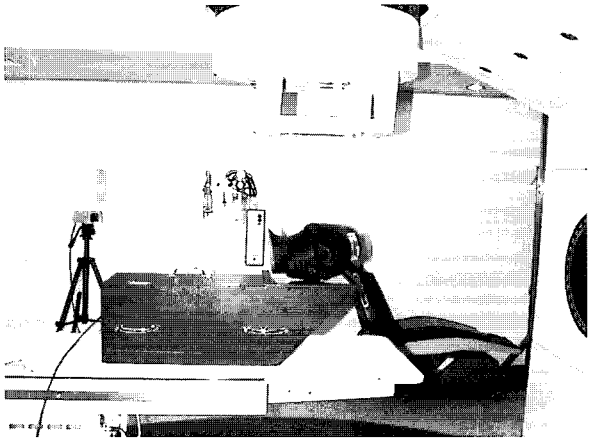

그림 3. 전자포탈영상장치 실험 과정
Fig. 3. Experimental setting of prototype CCD-based EPID for measurement of humanoid head phantom images in the 6MV LINAC

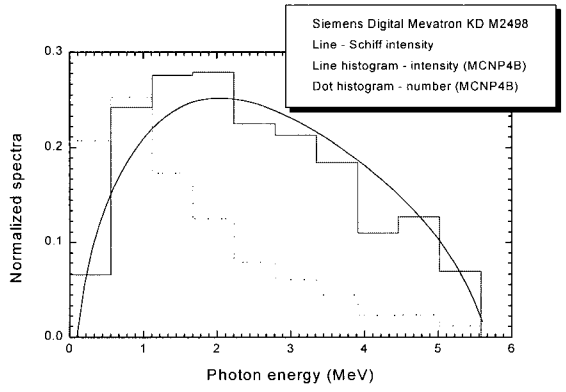

그림 4. 제동복사선의 스펙트럼 계산치
Fig. 4. Simulated bremsstrahlung spectra, number (dot histogram) and intensity (line histogram) and Schiff intensity (line) spectrum were represented

RESULTS AND DISCUSSIONS

1. Bremsstrahlung Spectrum

Simulated bremsstrahlung spectra, number and intensity and Schiff intensity spectrum were represented. (Fig.4) The mean energy of the bremsstrahlung x-ray is 1.57 MeV. As shown in Fig.4, the Monte Carlo simulation result provides reasonable agreement with a theoretical model and may be useful for applications in which the exact spectrum is not critical. The normalized number spectrum is, then, implemented to the source input of Monte Carlo simulation for estimating the detection efficiency of metal plate/phosphor screen detector.

2. Detection Efficiency

For the incident bremsstrahlung x-ray with the mean energy of 1.57MeV, the detection efficiency is shown in

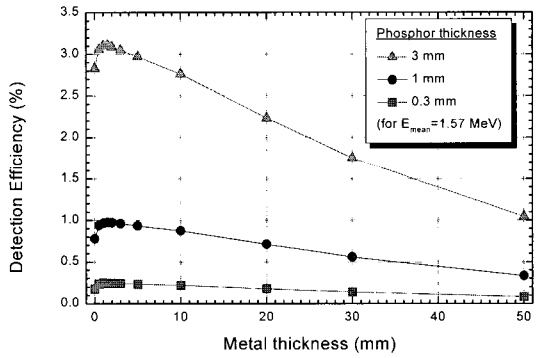

그림 5. 형광판의 계측효율
Fig. 5. Detection efficiency for 0.3, 1 and 3 mm-thick phosphor as a function of the metal thickness

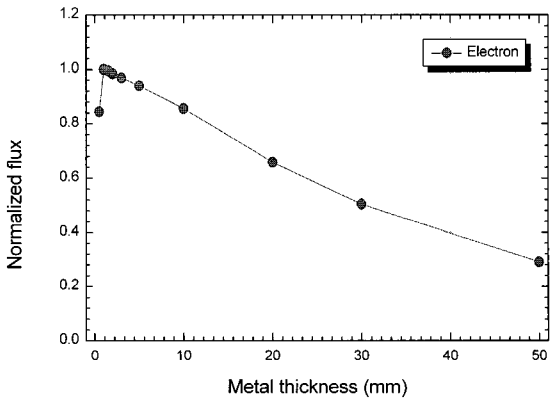

그림 6. 금속판에서 방출되는 전자속밀도
Fig. 6. Relative electron flux emitted from the metal plate as a function of metal thickness

Fig.5 in unit of percentage for the 0.3, 1, 3mm-thick phosphor screen as a function of the metal thickness. The result shows that, the detection efficiency rapidly approaches to the maximum value at a range of 1.5~2.0mm of metal thickness and then decreases very slowly as the metal thickness increases. This characteristic can be analyzed by using the electron flux shape emitted from the metal plate (Fig.6) and the electron path length in the phosphor screen. The number of electrons penetrating metal plate depends upon their energies and corresponding path lengths, so that the total absorbed energy distribution in the phosphor screen as a function of metal thickness shows a maximum value. The calculated detection efficiency was compared using experimental measurement result. Fig.7 shows the normalized light yields of calculation and measurement as a function of the metal thickness. The presence of the copper plate enhances the absorbed energy of the phosphor screen, particularly for the thinner phosphors. The phosphor screen is close to the electron equilibrium throughout its thickness if the metal is sufficiently thick. In other words, the metal plate increases the energy absorption of the 0.3mm-thick phosphor screen by about 10 times while for 3mm-thick phosphor screen the enhancement is only about 1.2 times. From this result, it was found that, the improvement of detection efficiency due to the metal plate is more effective, as the phosphor thickness is thinner.

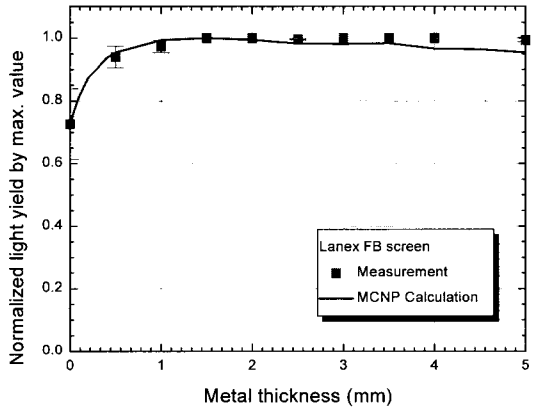

그림 7. 광량의 계산치와 실험치
Fig. 7. Normalized light yield by calculation and measurement as a function of metal thickness

3. Spatial Resolution

The distribution of the optical photon flux collected by $10\times10m^2$ pixel area on the free surface of the phosphor screen as function of the pixel position was calculated. Fig.8 shows the results for various phosphor thickness without metal plate, and Fig.9 represents the results for 1 mm-thick phosphor layer with various thickness of the metal plate. As shown in figures, it is observed that the spatial broadening is largely affected by the phosphor thickness but the metal plate could be negligible, in other words, the metal plate does not degrade the spatial resolution. From the results, it can be inferred that electrons emitted from metal plate is not significantly spread, but is well confined along the direction-line of the incident X-ray. Supplementary Monte Carlo simulation showed that 90% of electron flux emitted from the metal plates of thickness from 1 to 5mm is confined within the area of 1mm-diameter.

To quantify the spatial resolution, the edge spread function was fitted with the second-order exponentially decay curve as obtained from portal film. For comparing the measured edge spread function and the calculated

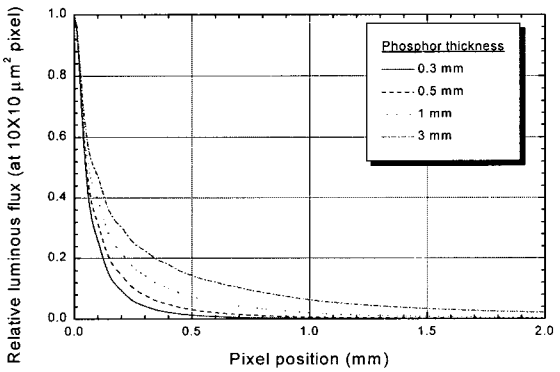

그림 8. 금속판이 없을 때 형광판 두께에 따른 빛의 퍼짐
Fig. 8. Relative distributions of optical photon flux as a function of position for various thickness of phosphor without the metal plate

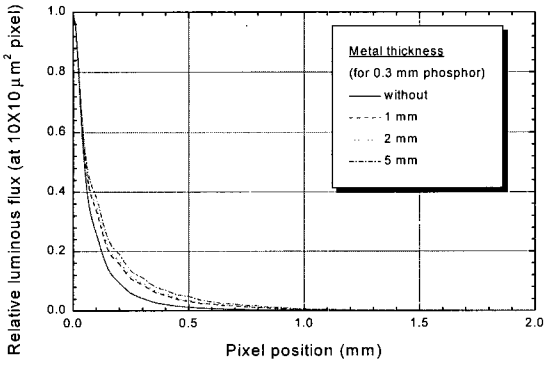

그림 9. 금속판 두께에 따른 빛의 퍼짐
Fig. 9. Relative distributions of optical photon flux as a function of position for various thickness of the copper plate with 0.3mm-thick phosphor screen

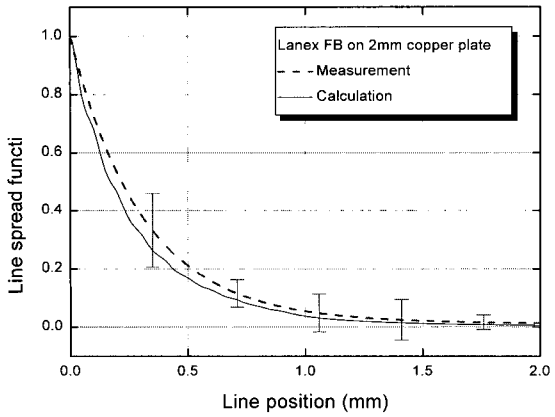

그림 10. 선퍼짐 함수의 계산치와 측정치
Fig. 10. Measured and calculated line spread functions of the 2mm-thick copper plate and the 0.3mm-thick phosphor screen

point spread function, these are converted into line spread functions by differentiation and integration, respectively. These two line spread functions are shown in Fig.10, and are agreed well to each other in error boundaries. The FWHMs of the line spread functions appear to be 0.342 mm and 0.436mm, for calculation and measurement, respectively. Unlike the calculation model, the phosphor screen is supported on a plastic support[21] and is bonded to the metal plate by plastic tapes so that the phosphor is not in direct contact with the metal plate in measurement. And also the scattering effects of the incident x-ray by surrounding materials including the film cassette were not considered in calculation. Since the high energy electrons emitted from the metal plate can spread in the plastic support and tapes before entering the phosphor and the film can be exposed by the scattered radiation, so that the measured FWHM is lager than the calculated one.

4. Acquired Images and Frame Averaging Method

In this experiment, 60 frames of images were acquired in video speed of 30 frames per second. As shown in Fig.11(a), an acquired single-frame image suffers notorious quantum noise, which is due to the counting statistics of the incident x-rays, the conversion fluctuations of x-rays into light quanta in x-ray detector and signal formation fluctuations in CCD camera[22]. The quantum noise can be largely reduced by the frame averaging method and Fig.11(b) shows the image which was acquired after 60 frames averaging. As the number of averaged frames increases, SNR (Signal-to-Noise Ratio) increases. At 60 frames averaged image, SNRs are increased by 10 and 17times for the skull and neck region, respectively. In addition, between the sampled areas, the image contrast rapidly increases as the number of frames averaged increases, and then starts to saturate at around 8 frames. (Fig. 12)

CONCLUSION

The detection efficiency as well as the spatial resolution for various combinations of metal plate /phosphor screen as a detector of video camera-based EPID were estimated by calculations and verified by the experimental measurements. The results show that, the detection efficiency is maximized by use of the 1.5~2.0mm-thick metal plate, and is slowly decreased as the metal thickness increases over 2mm. And it was found that the detection efficiency strongly depends on the emitting electron flux from the metal plate. The spatial resolution is degraded

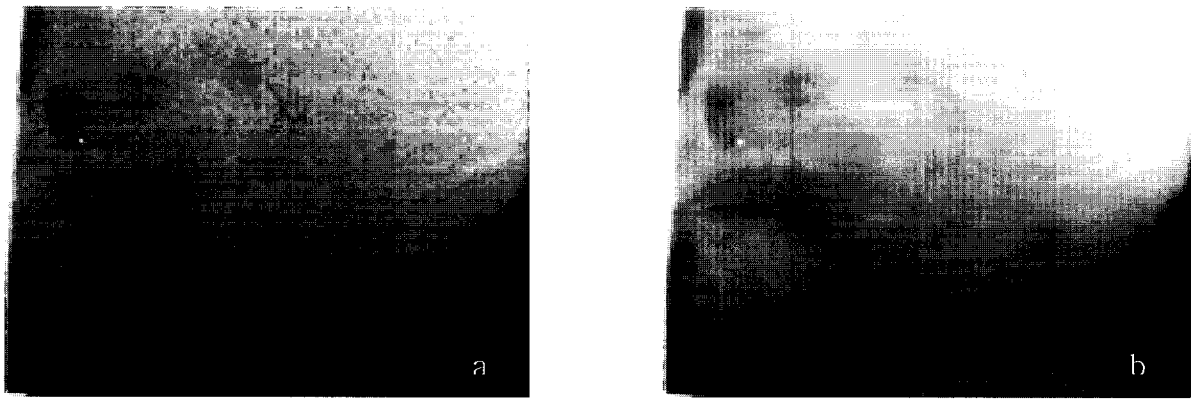

그림 11. 획득된 영상. (a) 1 프레임 영상 (b) 60 프레임의 평균 영상
Fig. 11. Acquired images from prototype CCD-based EPID. (a) A single video frame image containing serious quantum noise, (b) 60 frames averaged image, which shows quite removed quantum noise

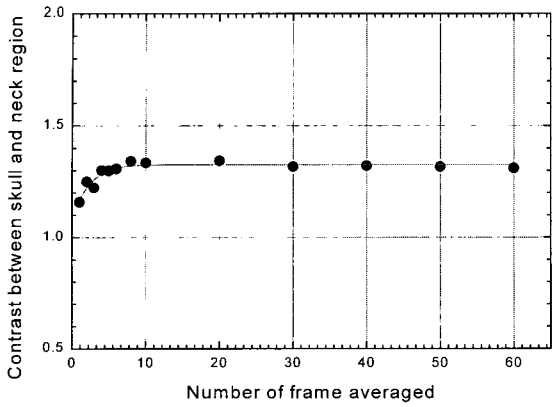

그림 12. 평균 프레임수에 따른 대조도
Fig. 12. Image contrast for small ROIs, between skull and neck region, of head-phantom as a function of averaged frame numbers

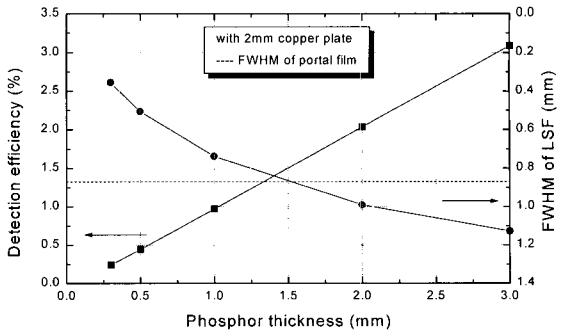

그림 13. 계측효율과 공간분해능
Fig. 13. The detection efficiency within the phosphor screen and FWHM of line spread function with the 2 mm-thick copper plate as a function of the phosphor thickness

as the phosphor thickness increases, but the degradation of the spatial resolution due to the metal plate can be negligible because of the strong directionality of electrons. It was revealed that the detection efficiency and the spatial resolution were mainly determined by the thickness of metal plate and phosphor screen, respectively.

Since the optimal thickness of the metal plate is 1.5~2.0mm, the detection efficiency and the spatial resolution have compromise in terms of the thickness of the phosphor screen. As the phosphor thickness increases, the detection efficiency increases but the spatial resolution decreases. The curve illustrating the trade-off between the detection efficiency and the spatial resolution of the metal plate/phosphor screen was obtained as a function of the thickness of phosphor screen with the 2mm-thick copper plate. (Fig.13) The spatial resolution of the portal film is 0.87mm, and the lowest detection efficiency of commercially used x-ray detector of EPID is 0.24%. This curve can be used to determine the optimal thickness of metal plate/phosphor screen as the x-ray detector of electronic portal imaging system as well as another imaging system using the similar detector structure.

The prototype CCD-based EPID with FOV of 20×20 cm^2 was developed and therapeutic x-ray radiographs were acquired. Although, in the interlaced mode, the captured image suffered from serious quantum noise, the quantum noise was reduced by frame averaging method. The frame averaging method improved the SNR and the image contrast. In order to reduce the quantum noise and to improve the image quality in therapeutic x-ray imaging application, the frame averaging is necessarily required.

REFERENCES

1. C.Williams, *All about cancer*, John Wiley and Sons, 1984
2. C.J.Karzmark, *Medical electron accelerators*, Mc-Graw-Hill.Inc., 1993
3. I.Rabinowitz, J.Broomberg, M.Goitein, Accuracy of radiation field alignment in clinical practice, I.J.Radiat. Oncol. Biol. Phys., Vol 11,p1857-1867, 1985
4. A.Dutreix, When and how can we improve precision in radiotherapy?, Radiother. Oncol., Vol 2, p275-292, 1984
5. P.Munro, J.A.Rawlinson, A.Fenster, A digital fluoroscopic imaging device for radiotherapy localization, I.J.Radiat. Oncol. Biol. Phys., Vol 18, p641-649, 1990
6. J.Leong, Use of digital fluoroscopy as an on-line verification device in radiation therapy, Phys. Med. Biol., Vol. 31, p985-992, 1986
7. A.G.Visser, H.Huizenga, V.G.M.Althof, et.al., Performance of a prototype fluoroscopic radiotherapy imaging system, I.J.Radiat. Oncol. Biol. Phys., Vol 18, p43-50, 1990
8. P.Munro, Portal imaging technology : past, present, and future, Seminars in radiation oncology, Vol 5, p115-133, 1995
9. T.Radcliffe, G.Barnea, B.Wowk, et.al., Monte Carlo optimization of metal/phosphor screens at megavoltage energies, Med. Phys., Vol 20, p1161-1169, 1993
10. P.Metcalfe, T.Kron, P.Hoban, *The physics of radiotherapy x-rays from linear accelerator*, Medical physics publishing, 1997
11. G.E.Desorby, A.L.Boyer, Bremsstrahlung review : An

analysis of the Schiff spectrum, Med. Phys., Vol. 18, p497-505, 1991

12. J.J.DeMarco, T.D.Solberg, R.E.Wallace, J.B.Smathers, A verification of the Monte Carlo code MCNP for thick target bremsstrahlung calculation, Med. Phys., Vol. 22, p11-16, 1995
13. J.F.Briesmeister, *MCNP-A General Monte Carlo N-Particle Transport Code, Version 4B*, LANL Report, LA-12625-M, 1997
14. D.A.Jaffray, J.J.Battista, A.Fenster, et.al., Monte Carlo studies of x-ray energy absorption and quantum noise in megavoltage transmission radiography, Med. Phys., Vol. 22, p1077-1088, 1995
15. R.K.Swank, Calculation of modulation transfer functions of x-ray fluorescent screens, Applied Optics, Vol. 12, p1865-1870, 1973
16. G.Lubberts, Random noise produced by x-ray fluorescent screens, J. Opt. Soc. Am., Vol. 58, p1475-1483, 1968
17. J.Bissonnette, P.Munro, Evaluation of a high-density scintillating glass for portal imaging, Med. Phy., Vol. 23, p401-406, 1996
18. G.E.Giakoumakis, C.D.Nomicos, P.X.Sandilos, Absolute efficiency of Gd_2O_2S:Tb screens under fluoroscopic conditions, Phy. Med. Biol., Vol. 34, p673-678, 1989
19. G.E.Giakoumakis, C.D.Nomicos, E.N.Yiakoumakis, et. al., Absolute efficiency of rare earth oxysulphide screens in reflection mode observation, Phy. Med. Biol., Vol. 35, p1017-1023, 1990
20. B.H.Hasegawa, *The physics of medical x-ray imaging*, Medical physics publishing, 1991
21. A.G.Haus, R.E.Dickerson, *Characteristics of screen-film combinations for conventional medical radiography*, Technical and scientific monograph, Eastman Kodak, 1995
22. R.Rajapakshe, S.Shalev, Noise analysis in real-time portal imaging. I. Quantization noise, Med. Phys, Vol. 21, p1263-1268, 1994